Journal of Renewable Materials

Tech Science Press

DOI: 10.32604/jrm.2022.016961

ARTICLE

Rapid Immobilization of Transferable Ni in Soil by $Fe_{78}Si_9B_{13}$ Amorphous Zero-Valent Iron

Liefei Pei, Xiangyun Zhang and Zizhou Yuan*

School of Materials Science and Engineering, Lanzhou University of Technology, Lanzhou, 730050, China

*Corresponding Author: Zizhou Yuan. Email: yuanzz@lut.edu.cn

Received: 11 April 2021 Accepted: 15 June 2021

ABSTRACT

Fe-Si-B amorphous zero-valent iron has attracted wide attention because of its efficient remediation of heavy metals and dye wastewater. In this paper, the remediation effect of amorphous zero-valent iron powder ($Fe_{78}Si_9B_{13}^{AP}$) on Ni contaminated soil was investigated. Results show that the immobilization efficiency of nickel in soil by $Fe_{78}Si_9B_{13}^{AP}$ with low iron content is higher than that by ZVI. The apparent activation energies of the reactions of $Fe_{78}Si_9B_{13}^{AP}$ with Ni^{2+} ions is 25.31 kJ/mol. After continuing the reaction for 7 days, Ni^{2+} ions is mainly transformed into monoplasmatic nickel (Ni^0) and nickel combined with iron (hydroxide) oxides. Microstructure investigations show that the product layer with nano-pore structure is beneficial to improve the reaction activity of $Fe_{78}Si_9B_{13}^{AP}$. After that, a magnetic separation process is introduced, in which part of the immobilized Ni are removed to reduce the total Ni content in soil by 58.21%. The results of simulated acid rain leaching experiment showed that the release of Ni in the soil after $Fe_{78}Si_9B_{13}^{AP}$ remediation is 62.89% lower than that before remediation.

KEYWORDS

Amorphous alloy; soil contamination; nickel; magnetic separation

1 Introduction

Soil is the most basic natural resource for human survival. Since the industrial revolution, the excessive exploitation of nickel ore and the widespread use of nickel-containing products have resulted in excessive nickel content in the soil environment [1,2]. Ni is one of the trace elements needed by organisms. It can stimulate the activity of some enzymes and plays a very important role in maintaining the normal metabolic activities of cells [3]. However, the demand of Ni for organisms is limited. If it exceeds a certain range, it will have a variety of toxic effects on organisms. Chami et al. [4] remediated Ni contaminated soil with sorghum and safflower. When the concentration of Ni was higher than 10 mg/kg, the growth of sorghum and safflower was seriously inhibited. Long-term accumulation of Ni in soil is difficult to degrade, causing economic loss and endangering human health at the same time [5,6]. In view of the strong biological toxicity of Ni, the World Health Organization lists it as a category I carcinogen.

The existence form of Ni in soil can be divided into immobilized Ni and mobile Ni. Immobilized Ni exists in the form of solid particles and is not absorbed by organisms, so it has little impact on the environment. However, mobile Ni has good solubility and fluidity, it is easy to enter the organism and

has a serious inhibitory effect on the growth of animals and plants [7–9]. From the perspective of ecological risk assessment, it has research value to transform the mobile Ni into a immobilized form with poor liquidity [10]. In recent years, researchers have used various organic and inorganic stabilizers to immobilize Ni in soil. For example, Shahbaz et al. [11] remediated Ni contaminated soil with zeolite (ZE). The results showed that the soil pH and cation exchange rate increased significantly after remediation. Ni was adsorbed on the surface of ZE, which effectively reduced the bioavailability of plants to Liu et al. [12] remediated Ni contaminated soil with acid-washed coconut shell biochar (MCSB) for 63 days and found that the soluble Ni in the soil was reduced by 57.2%, and the Ni in the immobilized soil could exist stably for a long time. It can be seen that immobilization has the advantages of low environmental harm, low energy consumption, and good stability in soil remediation.

At present, the commonly used soil remediation methods include in-situ chemical precipitation, adsorption, ions exchange and electrokinetic methods. Among them, immobilization remediation with cost-effective, less secondary pollution, and mature technology is considered to be the most effective way to eliminate the harm of heavy metals from contaminated soil [13,14]. The choice of stabilizer in the process of immobilization directly determines the effect of soil remediation. As we all know, the standard electrode potential of Ni is −0.23 V. In order to reduce soluble Ni^{2+} ions to Ni^{0} with poor mobility, it is necessary to choose a stabilizer with lower electronegativity. The standard electrode potential of Fe is −0.44 V and zero-valent iron (ZVI) has low cost. As an environmental functional material, it is widely used in the field of wastewater and soil remediation [15–17]. Madaffari et al. [18] used ZVI/lapillus to remove Ni in the column system. After 500 h of reaction, the removal rate of Ni reaches 99.9%. But only using ZVI as stabilizer, the removal efficiency is only 49%. The reason for this result is that the solid formation of Fe-Ni mixed hydroxide prevents Ni^{2+} ions from further contacting the unreacted ZVI surface, thereby hindering the further occurrence of redox reaction. In order to eliminate the phenomenon that traditional stabilizers are easy to be passivated, it is urgent to find new remediation materials with high reaction activity and low environmental harm.

Amorphous alloy (MGs) with atomic disorderly stacked structure has always been a hot spot in the field of alloy materials [19]. The MGs is a complex structure of multi-body mutual effects compared to the crystalline alloy arranged in the atomic rules. The reason is that the special atoms and electronic structures make the entire system in thermodynamics [20,21]. In recent years, with the continuous expansion and deepening of MGs in various application research fields, it shows efficient degradation performance in the treatment of environmental pollutants. Previous studies have shown that the apparent reaction rate coefficient of Fe-based amorphous alloy in the treatment of azo dye wastewater is 36 times that of crystalline alloy with the same component and 89 times that of ZVI [22]. Yan et al. [23] found that the degradation rate of Cu^{2+} in solution by Fe-based amorphous alloy strips can reach 99% within 60–100 min, but the degradation effect of ZVI on Cu^{2+} is not ideal. This is due to the existence of the "liquid-like" layer on the surface of MGs, which makes the surface diffusion rate much higher than that of crystalline alloy, which means that the surface of MGs has ultra-high reactivity [24–26]. Therefore, MGs with high reaction activity is becoming a new functional material with great advantages in the field of energy conversion catalysts.

In view of the fact that ZVI is prone to passivation in the reaction with pollutants, metastable material $Fe_{78}Si_9B_{13}{}^{AP}$ was used to remediate high concentration nickel contaminated soil and the remediation effect was compared with that of ZVI. The morphological transformation and reaction mechanism of Ni was studied. Further recovery of residual stabilizer particles and immobilized Ni by magnetic separation technology. This study expands the engineering application of amorphous alloys and provides a new method for in-situ remediation of heavy metal contaminated soils.

2 Materials and Methods

2.1 Materials

All chemicals employed in this study, including $NiSO_4 \cdot 6H_2O$, HCl, $MgCl_2$, CH_3COONa, HNO_3, CH_3COONH_4, CH_3COOH, H_2O_2, $NH_4OH \cdot HCl$, and NaOH were of analytical grade. ZVI was purchased from China Zhongye Chemicals Co. Ltd., Hebei China, which had a mean grain size (d_{50}) of ~1 μm. The purchase price is CNY 0.74/g. $Fe_{78}Si_9B_{13}{}^{AP}$ was purchased from Jiangsu Chuangling Chemicals Co., Ltd., Jiangsu China, which had a mean grain size (d_{50}) of ~10 μm. The price is CNY 0.77/g.

2.2 Soil Preparation

2.2.1 Soil Sampling

The loess uncontaminated by Ni was collected from Lanzhou University of Technology in Lanzhou City, Gansu Province, and the soil samples were screened by 2 mm sieve. In order to avoid the interference of soluble ions on the experimental results, the screened loess was eluted twice with 0.1 mol/L HCl solution. After drying and screening the loess mud, the soil samples needed for the experiment were obtained.

2.2.2 Preparation of Ni Contaminated Soil

The soil environmental quality risk control standard for soil contamination of development land stipulates that if the content of Ni in the soil exceeds 200 mg/kg, it is considered to be seriously polluted soil [27]. It has been reported that the maximum content of Ni in farmland around Jinchang city, known as the "nickel capital of China", is 577 mg/kg [28]. Therefore, the initial content of Ni in this experiment was selected as 600 mg/kg. 1 L $NiSO_4 \cdot 6H_2O$ solution with Ni^{2+} ions concentration of 600 mg/L was mixed with 1 kg dried soil and mechanically stirred until air dried. In order to ensure the uniform dispersion of Ni in soil, the concentration of Ni^{2+} ions was determined when different quality soil samples were added to the same stagnant water. The results showed that the concentration of Ni^{2+} ions was proportional to the number of soil samples, indicating that Ni^{2+} ions had good dispersion in soil.

2.3 Immobilization of Ni^{2+} Ions in the Soil

Soil remediation experiment is to evaluate the treatment effect of $Fe_{78}Si_9B_{13}{}^{AP}$ and ZVI on nickel contaminated soil at different temperatures. In order to avoid the influence of the surface oxide of the stabilizer on the experiment, the $Fe_{78}Si_9B_{13}{}^{AP}$ and ZVI were rinsed with 2% HCl before the experiment. The immobilization reaction was carried out in 10 jars, and the experimental conditions were exactly the same. 5 g of the Ni contaminated soil mentioned above were added to each jar, and the $MgCl_2$ solution of 50 mL 0.01 mol/L was added to each jar to reduce the non-specific adsorption of Ni^{2+} ions by the soil. Adjust the pH of the soil suspension to 6 with NaOH and HCl. According to the method of Shaaban et al. [29], pH meter (Delta320, Mettler Toledo instrument) was used to measure the pH of the soil suspension when the soil-water ratio (g/mL) was 1:10. In most experiments, the increase of the amount of stabilizer is beneficial to the improvement of immobilization efficiency [30]. However, when the concentration of Fe in soil is more than 5%, it will have a serious impact on plant growth [31]. Therefore, on the premise of ensuring the sufficient stabilizer needed for the reaction, the stabilizer dosage was selected as 0.25 g to add to the jar and placed in the vibration box. When the reaction time was 0.5, 1, 2, 4, 5, 10 and 20 h, the 10 mL slurry was extracted from one of the jars and centrifuged at a high speed by a centrifuge, the filtered supernatant was injected into a 10 mL centrifuge tube with 0.45 μm cellulose acetate syringe filters. The residual slurry was extracted using the steps described by Ure et al. [32], and the concentrations of various forms of Ni were determined by inductively coupled plasma atomic emission spectrometry (ICP-AES). It should be noted that the remaining two bottles of slurry continued to react until the seventh day after 20 h of reaction, in order to provide sufficient time for the morphological transformation of Ni in the soil. Seven days later, one bottle of slurry was remediated

according to the above extraction method. The other part of the slurry was used to separate ferromagnetic ZVI and Ni particles: A magnet (~100 mT) wrapped in plastic films were in close contact with the amended soil and move back and forth, and ferromagnetic particles were attracted by magnets to attach to the film [33]. Remove the film from the magnet and the ferromagnetic particles were separated from the magnet again. The separated particles were washed with deionized water. Repeat several times until the ferromagnetic particles cannot be separated. The selected samples were dissolved in acid to determine the total Fe and Ni recovered. Table 1 shows the reagents and reaction conditions used in the continuous extraction of metals in the soil.

Table 1: extraction of nickel in soil

	Forms	Reagents
SE	Bioavailable	1 mol/L $MgCl_2$, 0.11 mol/L CH_3COOH
OX	Reducible	0.5 mol/L $NH_4OH{\cdot}HCl$
OM	Oxidizable	9.79 mol/L H_2O_2, 1 mol/L CH_3COONH_4
RE	Residual	HCl:HNO_3, 1:3 v/v

In order to determine the immobilization effect of stabilizers on Ni^{2+} ions, the immobilization rate (η) was calculated by Eqs. (1) and (2).

$$C_t = 600 \times w_{SE}, \tag{1}$$

$$\eta = (1 - C_t/C_0) \times 100\%, \tag{2}$$

where C_t is the current concentration of bioavailable Ni (SE); C_0 is the initial concentrations of SE. In order to compare and analyze the immobilization rate of Ni^{2+} ion by $Fe_{78}Si_9B_{13}{}^{AP}$ and ZVI, the experimental results were fitted by quasi-first-order kinetic Eq. (3) linear fitting.

$$C_t/C_0 = C_1 exp(-t/t_0) + C_2, \tag{3}$$

where C_1 and C_2 are constants; t is the reaction time; t_0 is the reaction time constant.

Activation energy (ΔE) reflects the difficulty of chemical reaction to a certain extent. ΔE can be obtained by fitting the time constant t_T obtained at different temperatures according to Arrhenius-type Eq. (4).

$$t_T = A exp(-\Delta E/RT), \tag{4}$$

2.4 Soil Column Leaching Experiment with Simulated Acid Rain

In order to investigate the long-term stability of immobilized Ni in the soil after $Fe_{78}Si_9B_{13}{}^{AP}$ remediation, the soil was leached with acid solution before and after remediation. The pH value and leaching volume of acid rain were designed according to the nature and precipitation of acid rain in Lanzhou [34]. In the experiment, the pH value of simulated acid rain solution is 5, and the molar concentration ratio of H_2SO_4 to HNO_3 is 4:1. The experimental leaching column device is shown in Fig. 1. The leaching column was a cylindrical PVC tube with an inner diameter of 5 cm. Silica sand with a height of about 2 cm was placed at the bottom of the column, covered with two layers of medium-speed qualitative filter paper, and then filled with about 500 g remediated soil with the bulk density of 1.3 g/cm^3. To prevent the soil sample from spattering during leaching, a layer of filter paper was laid on the soil. According to statistics, the average annual rainfall in Lanzhou is about 330 mm, and the actual

leaching volume is 650 mL relative to this column. Under the control of the peristaltic pump, the simulated rain liquid was slowly sprayed from the top of the column at the speed of 5 mL/min. In order to make the soil have a sufficient reaction time, every time the 650 mL solution was leached, the soil was stabilized for 12 h before the next leaching, then leached for 5 times, which was equivalent to 5 years of precipitation. The concentration of Ni^{2+} ions in the leachate was determined by ICP-AES. The leaching process of unremediated contaminated soil was completely consistent with the above steps.

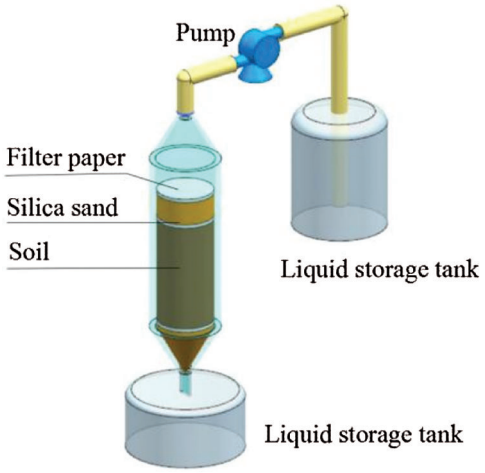

Figure 1: Experimental equipment for simulated acid rain leaching

3 Results and Discussion

3.1 Characterization of $Fe_{78}Si_9B_{13}^{AP}$ and ZVI

The structure and morphology of $Fe_{78}Si_9B_{13}^{AP}$ and ZVI were distinguished by XRD and SEM before reaction. As shown in Fig. 2a, the electron diffraction pattern of $Fe_{78}Si_9B_{13}^{AP}$ shows a diffuse halo peak around $2\theta = 45°$, and no crystallization peaks are detected in the rest, which is a typical iron-based amorphous alloy spectrum. In the electron diffraction pattern of ZVI, there is only α-Fe phase and no diffraction peak of iron oxide, which indicates that ZVI has high purity. Meanwhile, there are neither lattice stripes nor lattice diffraction spots in Fig. 2b, which further confirms $Fe_{78}Si_9B_{13}^{AP}$ has an amorphous structure. Figs. 2c and 2d are SEM images of $Fe_{78}Si_9B_{13}^{AP}$ and ZVI. The results show that the powders prepared by atomization are spherical particles with smooth surface and no obvious agglomeration. The diameters of $Fe_{78}Si_9B_{13}^{AP}$ are 40–50 μm, and the diameters of ZVI are 1–3 μm.

3.2 Immobilization of Ni^{2+} Ions in the Soil by $Fe_{78}Si_9B_{13}^{AP}$ and ZVI

Figs. 3a and 3b show the fitting curve of concentration of soluble Ni^{2+} ions during immobilization by $Fe_{78}Si_9B_{13}^{AP}$ and ZVI at 293, 303, 313 and 323 K. With the progress of the immobilization reaction, the normalized concentration decreases exponentially, and each reaction reach equilibrium within 10 h. When the reaction time is extended to 48 h, there is no secondary dissolution of Ni^{2+} ions, which indicate that the reaction product could exist stably. In order to further study each reaction rate, the pseudo first-order kinetic equation (Eq. (3)) is used to fit the experimental results to obtain t_0 as shown in Fig. 3c. t_0 indicates the time it takes when the concentration of Ni^{2+} ions decreases to 1/e of the initial concentration, which can indirectly reflect the immobilization rate of Ni^{2+} ions by the two materials. When the concentration of Ni^{2+} ions is 60 mg/g and the dosage of $Fe_{78}Si_9B_{13}^{AP}$ is 5 g/kg, the t_0 obtained under the experimental conditions of 293, 303, 313 and 323 K is 2.55, 2.41, 1.92 and 1.31 h, respectively. Under the same conditions, the t_0 obtained by using ZVI as stabilizer is 24.15, 15.51, 10.8,

and 7.26 h, respectively. It can be seen that when the same amount of Ni^{2+} ions is immobilized under the same experimental conditions, $Fe_{78}Si_9B_{13}{}^{AP}$ takes less time than ZVI. In other words, the reaction rate of $Fe_{78}Si_9B_{13}{}^{AP}$ with Ni^{2+} ions is much higher than that of ZVI. Fig. 3d shows the change of the immobilization rate of the stabilizers at each temperature calculated by Eq. (2). The immobilization rate of different experimental group increases with the increase of temperature. When the temperature is 293, 303, 313 and 323 K, the immobilization rate of Ni^{2+} ions by $Fe_{78}Si_9B_{13}{}^{AP}$ is 80%, 82%, 84%, and 85%, respectively. However, the immobilization rate of ZVI to Ni^{2+} ions is relatively low, which is only 64%, 70%, 72%, and 74%, respectively. Obviously, At the same temperature, the immobilization rate of Ni^{2+} ions by $Fe_{78}Si_9B_{13}{}^{AP}$ is much higher than that of ZVI. Normally, the large specific surface area and high content of reactants are beneficial to the reaction [35]. However, the experimental results are not the case. The reaction rate of amorphous alloys with smaller specific surface area and lower iron content is higher than that of ZVI with larger specific surface area and higher iron content, which may be due to the thermodynamic instability of amorphous alloys.

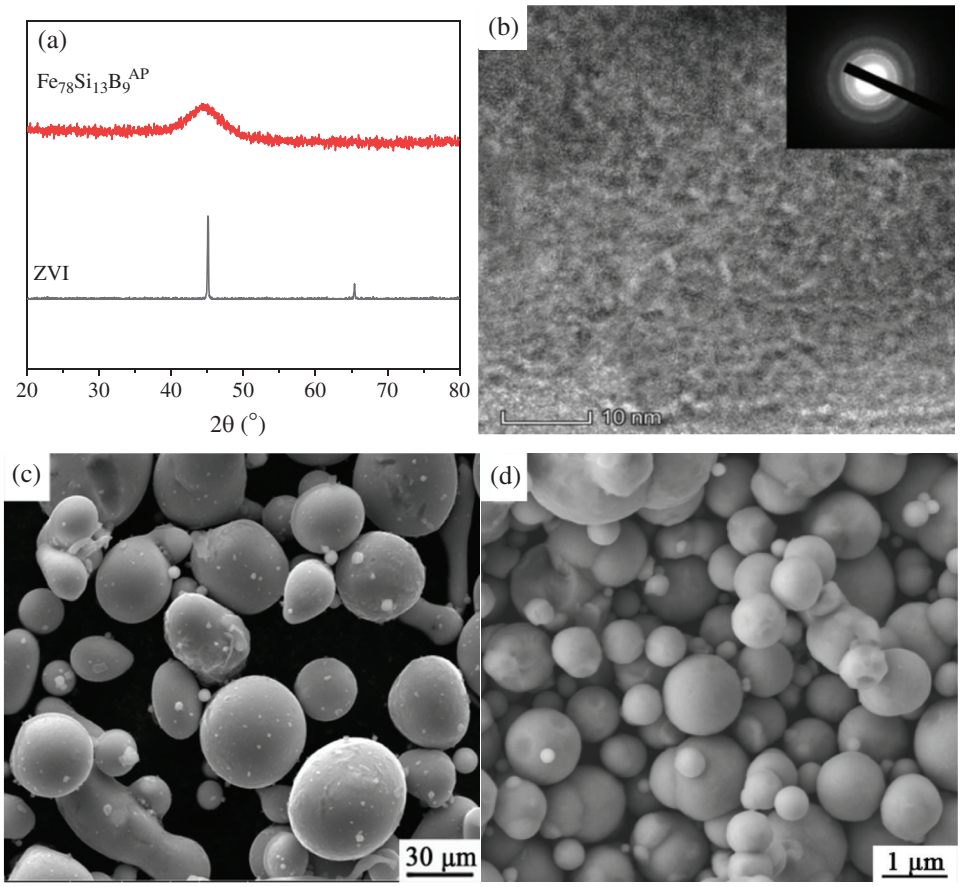

Figure 2: (a) The XRD patterns of the ZVI and $Fe_{78}Si_9B_{13}{}^{AP}$; (b) The TEM image of the $Fe_{78}Si_9B_{13}{}^{AP}$; (c) and (d) The SEM image of the $Fe_{78}Si_9B_{13}{}^{AP}$ and ZVI, respectively

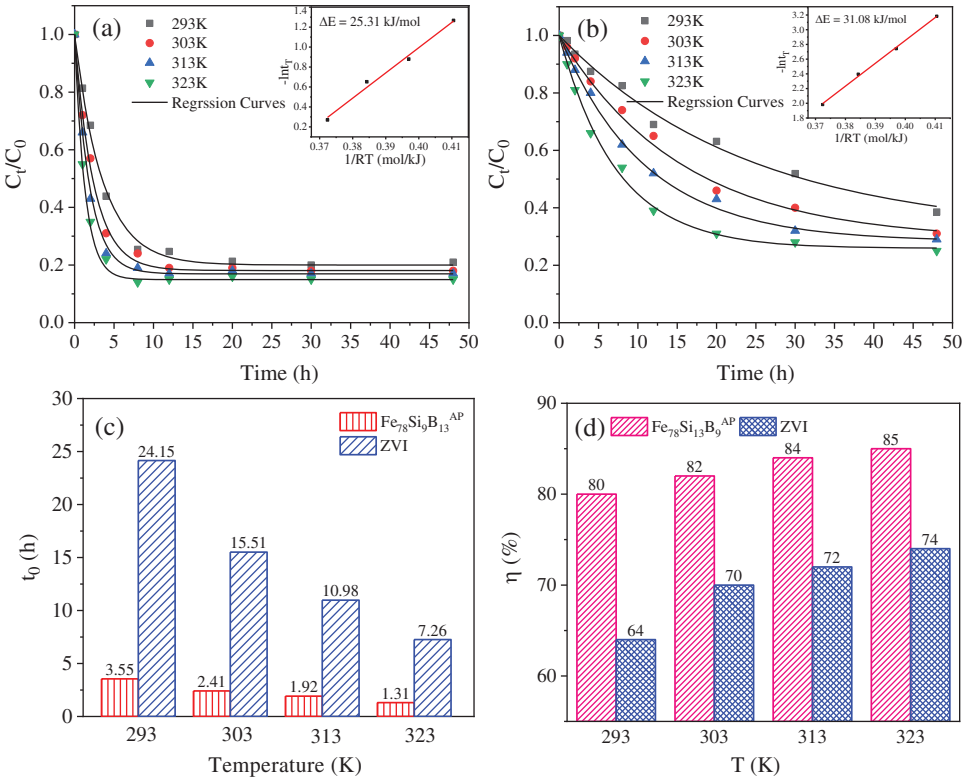

Figure 3: The curve of the normalized concentration of soluble Ni^{2+} ions during immobilization by $Fe_{78}Si_9B_{13}{}^{AP}$ (a) and ZVI (b); (c) the time constants t_0 at different temperatures; (d) immobilization rate

Activation energy (ΔE) can reflect the difficulty of chemical reaction to a certain extent [36]. In order to further explore the deep reason why amorphous $Fe_{78}Si_9B_{13}{}^{AP}$ has high activity, the reaction activation energies of $Fe_{78}Si_9B_{13}{}^{AP}$ and ZVI are obtained by Eq. (4) fitting. As shown in the inserts in Figs. 3a and 3b, the ΔE of $Fe_{78}Si_9B_{13}{}^{AP}$ and ZVI are 25.31 kJ/mol and 31.08 kJ/mol, respectively. Compared with ZVI, $Fe_{78}Si_9B_{13}{}^{AP}$ has lower ΔE. This is due to the fact that amorphous alloys have higher Gibbs free energy, therefore, less energy is needed to transform from the stable state to the active state. In other words, $Fe_{78}Si_9B_{13}{}^{AP}$ is more likely to react with Ni^{2+} ions [37]. This also explains why $Fe_{78}Si_9B_{13}{}^{AP}$ has a faster reaction rate. Compared with the activation energy of general chemical reaction (60–250 kJ/mol) [38], the ΔE of the $Fe_{78}Si_9B_{13}{}^{AP}$ and ZVI in this experiment is relatively lower. From the point of view of reaction control link, ΔE at 8–21 kJ/mol indicates that the reaction is controlled by diffusion in solution, while the chemical reaction controlled by surface diffusion $\Delta E > 30$ kJ/mol [39]. The activation energy of $Fe_{78}Si_9B_{13}{}^{AP}$ is between 21–30 kJ/mol, indicating that the reactions are controlled by both solution diffusion and surface diffusion. For the ZVI with $\Delta E_{(ZVI)} > 30$ kJ/mol, although its iron content is higher than that of $Fe_{78}Si_9B_{13}$, the passivation film formed on the surface of ZVI during the reaction blocks the adsorption and movement of Ni^{2+} ions on the surface of ZVI, thus limiting the transfer of electrons from Fe to Ni^{2+} ions.

3.3 Changes of Nickel Fractions in Soil after Immobilized Remediation

In order to explore the form transformation of Ni in soil and determine the immobilization effect of $Fe_{78}Si_9B_{13}{}^{AP}$ and ZVI on transformable Ni, the soil before and after treatment is continuously extracted by the method described by Ure et al. [32]. As shown in Fig. 4, the fraction of SE in the unremediated Ni contaminated soil accounted for 59.79% of the total, and the other forms of Ni are: 14.53% OX, 19.45%

OM, and 6.23% RE. After 200 h of treatment with $Fe_{78}Si_9B_{13}{}^{AP}$ and ZVI. The existence forms in soil are shown in Fig. 4: the fraction of SE in each experimental group decrease significantly, which indicate that the two kinds of iron-based materials have certain immobilization effect on Ni^{2+} ions. At the experimental temperature of 293, 303, 313 and 323 K, the fraction of SE in soil immobilized with $Fe_{78}Si_9B_{13}{}^{AP}$ decreased by 47.33%, 48.58%, 49.20%, and 50.45%, respectively. Obviously, the higher the temperature is, the more obvious the immobilization effect is. This is because the activity of the reactants increases with the increase of temperature, and it is easier for Ni^{2+} ions to obtain electrons that are reduced to immobilize Ni. In the control group, the fraction of SE with ZVI as stabilizer decreased by 38.26%, 41.34%, 42.33%, and 43.60%, respectively. It means that the content of movable Ni in ZVI immobilized soil is much higher than that in $Fe_{78}Si_9B_{13}{}^{AP}$ immobilized soil. By comparison, it is found that the fraction of immobilized Ni in the remediated soil also changed accordingly. The fraction of OX increases obviously, which is mainly due to the surface energy and structure of the iron oxides formed by the reaction are highly heterogeneous. The active sites with high energy and low coordination number have strong adsorption and can bind to Ni^{2+} ions [40]. Because hydrogen peroxide can not only decompose organic matter under acidic conditions, but also oxidize reduce Ni^0 to Ni^{2+} ions. The increase of the fraction of OM is mainly caused by the leaching of Ni^0. When the experimental temperature is 323 K, the fraction of Ni reduced by $Fe_{78}Si_9B_{13}{}^{AP}$ and ZVI are 44.38% and 31.45%, respectively. The process of transforming SE, OX, and OM into RE is relatively slow, so the fraction of RE is maintained at about 6%. At each experimental temperature, the fraction of SE in the soil remediated with $Fe_{78}Si_9B_{13}{}^{AP}$ is lower than that of ZVI. Considering the cost factor, the market price of $Fe_{78}Si_9B_{13}{}^{AP}$ and ZVI is similar (CNY~0.7/g), and the remediation effect of $Fe_{78}Si_9B_{13}{}^{AP}$ on contaminated soil is obviously better than that of ZVI, so $Fe_{78}Si_9B_{13}{}^{AP}$ can be used as a substitute for traditional remediation material ZVI in the field of soil or groundwater remediation.

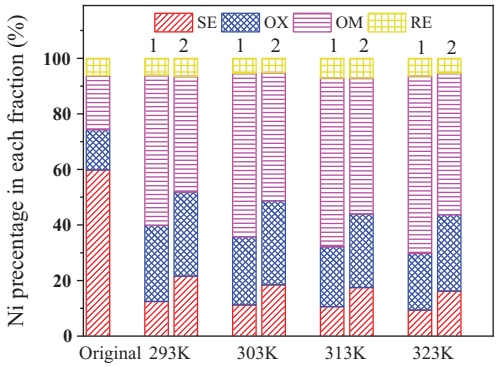

Figure 4: Changes of different fractions of nickel after immobilized remediation (1: $Fe_{78}Si_9B_{13}{}^{AP}$, 2: ZVI)

3.4 Reaction Mechanism Analysis

In order to explore the reasons for the obvious difference in the immobilization efficiency of Ni^{2+} ions by $Fe_{78}Si_9B_{13}{}^{AP}$ and ZVI, the surface morphology of the stabilizer after 200 h reaction is observed by SEM. In Fig. 5a, the surface of $Fe_{78}Si_9B_{13}{}^{AP}$ is severely corroded and a large number of nano-sized granular products are attached to the surface. Through the magnified image of regional (A) (Fig. 5b), the product structure can be further observed. The surface of the powder forms flower-shaped structure. Ni^{2+} ions can diffuse to the reaction interface through the triangular prismatic pores in the flower-shaped structure, which is beneficial to the reaction. Fig. 5c shows the product of the reaction of ZVI with Ni^{2+} ions. The reaction products are dendritic structures growing in different directions. To clearly observe the surface product of ZVI, the C region in Fig. 5c is enlarged and displayed in Fig. 5d. There is a product layer with thickness of about 200 nm and flocculent structure on the surface of ZVI, which hinders the diffusion of Ni^{2+} ions to the

reaction interface to some extent. Regarding the mechanism explanation that the difference in physical structure of the product layer between the amorphous alloy and the crystalline alloy causes the surface diffusion rate of the amorphous alloy to be much higher than the diffusion rate of the crystalline solid, the researchers believe that it is due to the existence of an "liquid-like" interface on the surface of $Fe_{78}Si_9B_{13}{}^{AP}$ [41]. Fig. 6 shows the XRD spectrum of the reaction products. The XRD curve of the $Fe_{78}Si_9B_{13}{}^{AP}$ shows that the Bragg peak of Ni^0 is superimposed on the broad halo peak, indicating that the reduced product of Ni^{2+} ions is Ni^0. The reaction only consumes the surface constituent atoms of the $Fe_{78}Si_9B_{13}{}^{AP}$ without changing its basic atomic structure. XRD pattern of the ZVI show sharp Bragg peaks of Ni^0, indicating the same remediation mechanism of the Ni^{2+} ions by $Fe_{78}Si_9B_{13}{}^{AP}$ and ZVI.

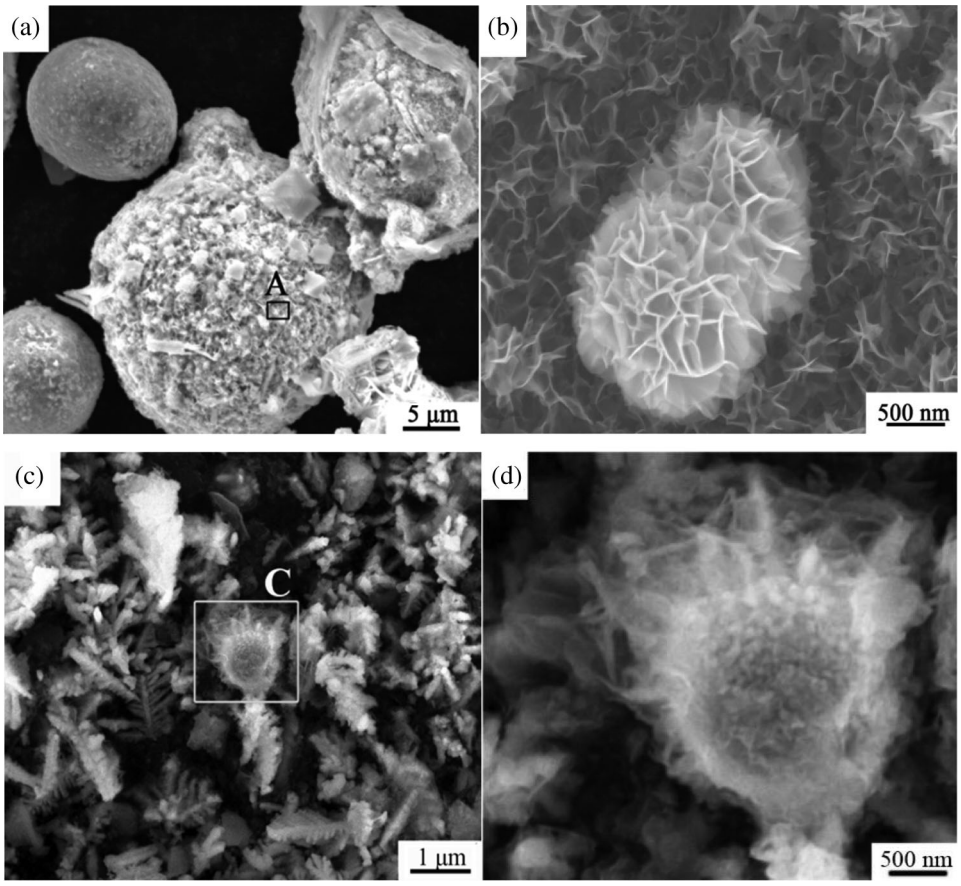

Figure 5: (a) The surface morphology of $Fe_{78}Si_9B_{13}{}^{AP}$; (b) The magnified image of regional (A); (c) The surface morphology of ZVI; (d) The magnified image of regional (C)

3.5 Magnetic Separation

Although $Fe_{78}Si_9B_{13}{}^{AP}$ and ZVI can effectively reduce mobile Ni^{2+} ions, the immobilized Ni can not be degraded. When the soil pH or redox conditions change, the immobilized Ni has the potential risk of transforming into mobile Ni^{2+} ions. On the other hand, the residual iron-based alloy may also adversely affect the soil structure and biological community [42]. As shown in Fig. 7, the feasibility of this method is verified. The magnetic separation rate of Fe can reach up to 76.25% after ZVI treatment. The iron recovery rate of $Fe_{78}Si_9B_{13}{}^{AP}$ treatment is about 60%, and the total remaining iron content in the soil is less than the limit value 50 g/kg. However, the result of magnetic separation of Ni is not ideal. The magnetic separation rate of Ni by $Fe_{78}Si_9B_{13}{}^{AP}$ is up to 58.21%, and the content of residual total Ni in

the soil is 250.8 mg/kg, which is slightly higher than the upper limit 200 mg/kg of Ni contaminated soil stipulated by the state. This shows that the efficient immobilization of Ni^{2+} ions by $Fe_{78}Si_9B_{13}{}^{AP}$ does not mean that ferromagnetic Ni can be completely separated from soil. As can be seen from Fig. 4, the immobilization remediation of soil by $Fe_{78}Si_9B_{13}{}^{AP}$ should contain 20.41% OX and 44.38% Ni^0 at 323 K. That is, 64.79% of Ni can be magnetically selected in theory. However, the difference between the experimental value and the theoretical value is 6.52%, which may come from the adsorption of soil to Ni. In view of the low magnetic separation rate of Ni, some researchers think that it is very important to enhance the binding between the product and the stabilizer [33]. In contrast, the highest magnetic separation rates of Ni in ZVI remediated soils is only 39.36%. The contents of residual total Ni in soil are 363.84 mg/kg, which are much higher than the upper limit of 200 mg/kg. From the above experimental results, it can be seen that $Fe_{78}Si_9B_{13}{}^{AP}$ combined with magnetic separation technology can significantly reduce the content of total Ni and Fe in soil without obvious damage to soil structure, which is a soil remediation method for energy saving and environmental protection.

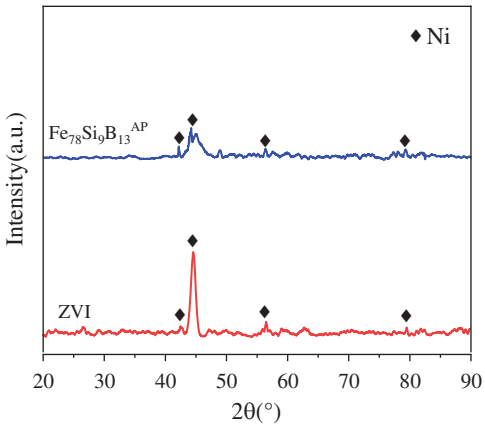

Figure 6: XRD spectrum of the reaction products

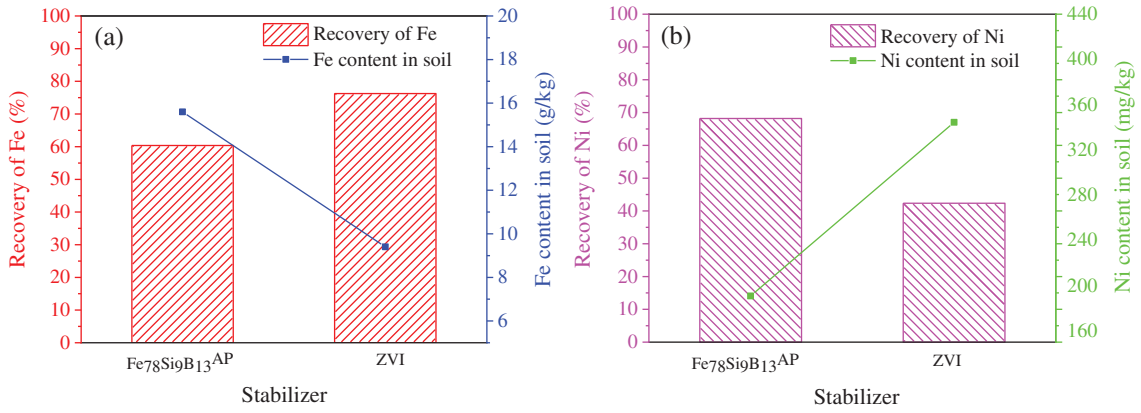

Figure 7: The magnetic separation rate of Fe (a) and Ni (b) from immobilization remediation of soil by $Fe_{78}Si_9B_{13}{}^{AP}$ and ZVI

3.6 Leaching with Simulated Acid Rain

In order to evaluate the stability of Ni in soil after $Fe_{78}Si_9B_{13}{}^{AP}$ remediation, artificial leaching of remediated soil and unremedied soil are carried out by simulated acid rain. Fig. 8 shows the cumulative

release of Ni from the soil after 5 times of simulated acid rain. In general, the cumulative release of Ni increased with the increase of the leaching cycle of simulated acid rain, and the third leaching cycle reached a maximum of 7.86 mg/kg, accounting for 1.31% of the total Ni content in the soil. This is due to the increase of H^+ ions content, on the one hand, desorption of Ni^{2+} adsorbed in the soil, on the other hand, H^+ ions dissolves the Ni^0 and iron (hydroxide) oxides to make the immobilized Ni dissolve again. After leaching for 3 times, there are almost no Ni^{2+} ions in the leachate. The maximum release of Ni from unremediated soil is 21.18 mg/kg, accounting for 3.53% of the total soil Ni. By comparison, it is found that the release of Ni in the soil remedied by $Fe_{78}Si_9B_{13}{}^{AP}$ decreased by 62.89%. Therefore, $Fe_{78}Si_9B_{13}{}^{AP}$ can effectively immobilize Ni^{2+} ions and reduce the potential risk of Ni in soil.

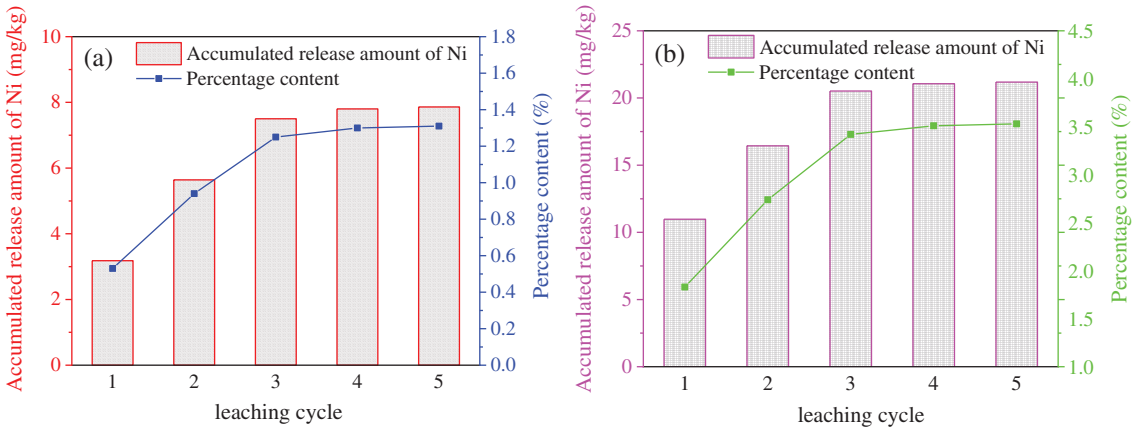

Figure 8: Accumulated release amount of Ni from soils under leaching with simulated acid rain: (a) non-remediated soils, (b) $Fe_{78}Si_9B_{13}{}^{AP}$-remediated soils

4 Conclusions

Compared with ZVI, the effects of $Fe_{78}Si_9B_{13}{}^{AP}$ with metastable structure on the remediation of soil containing high levels of Ni were discussed in this paper. It was found that $Fe_{78}Si_9B_{13}{}^{AP}$ can reduce and immobilize Ni^{2+} ions in soil faster and more effectively than ZVI. The immobilization rate of Ni^{2+} ions by $Fe_{78}Si_9B_{13}{}^{AP}$ is 11% higher than that by ZVI. This result can be attributed to $Fe_{78}Si_9B_{13}{}^{AP}$ having lower activation energy than ZVI, and loose product layer structure provides a channel for the movement of Ni^{2+} ions to the reaction interface. After that, the magnetic separation process further reduced the immobilized Ni in the soil by 58.21%. Finally, the acid rain leaching experiment confirms that the release of Ni in the soil after $Fe_{78}Si_9B_{13}{}^{AP}$ remediation is 62.89% lower than that before remediation. These findings prove that $Fe_{78}Si_9B_{13}{}^{AP}$ is a promising soil immobilization improver and expands the application range of amorphous alloys.

Acknowledgement: This work was supported by the National Natural Science Foundation of China (NSFC) [Grant Nos. 51661015 and 52061024]; and the Natural Science Foundation of Zhejiang Province [Grant No. LQ20E010002].

Funding Statement: This research was funded by the National Natural Science Foundation of China (NSFC) [Grant Nos. 51661015 and 52061024]; and the Natural Science Foundation of Zhejiang Province [Grant No. LQ20E010002].

Conflicts of Interest: The authors declare that they have no conflicts of interest to report regarding the present study.

References

1. Lian, H. L., Xiang, P., Xue, Y. H., Jiang, Y. Z., Li, M. Y. et al. (2020). Efficiency and mechanisms of simultaneous removal of microcystis aeruginosa and microcystins by electrochemical technology using activated carbon fiber/nickel foam as cathode material. *Chemosphere, 252,* 126431. DOI 10.1016/j.chemosphere.2020.126431.
2. Raval, N. P., Shah, P. U., Shah, N. K. (2016). Adsorptive removal of nickel(II) ions from aqueous environment: A review. *Journal of Environmental Management, 179(1),* 1–20. DOI 10.1016/j.jenvman.2016.04.045.
3. Yusuf, M., Fariduddin, Q., Hayat, S., Ahmad, A. (2011). Nickel: An overview of uptake, *Essentiality and Toxicity in Plants. Bulletin of Environmental Contamination & Toxicology, 86(1),*1–17. DOI 10.1007/s00128-010-0171-1.
4. Chami, Z. A., Amer, N., Bitar, L. A., Cavoski, I. (2015). Potential use of sorghum bicolor and carthamus tinctorius in phytoremediation of nickel, lead and zinc. *International Journal of Environmental Science & Technology, 12,* 3957–3970. DOI 10.1007/s13762-015-0823-0.
5. Siddiqui, M. N., Ali, I., Asim, M., Chanbasha, B. (2020). Quick removal of nickel metal ions in water using asphalt-based porous carbon. *Journal of Molecular Liquids, 308,* 113078. DOI 10.1016/j.molliq.2020.113078.
6. Es-Sahbany, H., Berradi, M., Nkhili, S., Hsissou, R., Allaoui, M. (2019). Removal of heavy metals (nickel) contained in wastewater-models by the adsorption technique on natural clay. *Materials Today: Proceedings, 13,* 866–875. DOI 10.1016/j.matpr.2019.04.050.
7. Georgieva, V. G., Gonsalvesh, L., Tavlieva, M. P. (2020). Thermodynamics and kinetics of the removal of nickel (II) ions from aqueous solutions by biochar adsorbent made from agro-waste walnut shells. *Journal of Molecular Liquids, 312,* 112788. DOI 10.1016/j.molliq.2020.112788.
8. Islam, M. A., Awual, M. R., Angove, M. J. (2019). A review on nickel(II) adsorption in single and binary component systems and future path. *Journal of Environmental Chemical Engineering, 7(5),* 103305. DOI 10.1016/j.jece.2019.103305.
9. Zhu, Y., Fan, W., Zhou, T., Li, X. (2019). Removal of chelated heavy metals from aqueous solution: A review of current methods and mechanisms. *Science of the Total Environment, 678(15),* 253–266. DOI 10.1016/j.scitotenv.2019.04.416.
10. Gong, Y., Zhao, D., Wang, Q. (2018). An overview of field-scale studies on remediation of soil contaminated with heavy metals and metalloids: Technical progress over the last decade. *Water Research, 147,* 440–460. DOI 10.1016/j.watres.2018.10.024.
11. Shahbaz, A. K., Lewińska, K., Iqbal, J., Ali, Q., Rahman, M. et al. (2018). Improvement in productivity, nutritional quality, and antioxidative defense mechanisms of sunflower (*Helianthus annuus* L.) and maize (*Zea mays* L.) in nickel contaminated soil amended with different biochar and zeolite ratios. *Journal of Environmental Management, 218(218),* 256–270. DOI 10.1016/j.jenvman.2018.04.046.
12. Liu, H., Xu, F., Xie, Y., Wang, C., Zhang, A. et al. (2018). Effect of modified coconut shell biochar on availability of heavy metals and biochemical characteristics of soil in multiple heavy metals contaminated soil. *Science of the Total Environment, 645,* 702–709. DOI 10.1016/j.scitotenv.2018.07.115.
13. Theodoratos, P., Papassiopi, N., Xenidis, A. (2002). Evaluation of monobasic calcium phosphate for the immobilization of heavy metals in contaminated soils from lavrion. *Journal of Hazardous Materials, 94(2),* 135–146. DOI 10.1016/S0304-3894(02)00061-4.
14. Zheng, L., Wang, W., Shi, Y. (2010). The effects of alkaline dosage and Si/Al ratio on the immobilization of heavy metals in municipal solid waste incineration fly ash-based geopolymer. *Chemosphere, 79,* 665–671. DOI 10.1016/j.chemosphere.2010.02.018.
15. Cao, M., Tu, S., Xiong, S., Zhou, H., Chen, J. et al. (2018). EDDS enhanced PCB degradation and heavy metals stabilization in co-contaminated soils by ZVI under aerobic condition. *Journal of Hazardous Materials, 358,* 265–272. DOI 10.1016/j.jhazmat.2018.06.056.
16. Liu, Y., Wang, J. (2019). Reduction of nitrate by zero valent iron (ZVI)-based materials: A review. *Science of the Total Environment, 671,* 388–403. DOI 10.1016/j.scitotenv.2019.03.317.
17. Zhao, X., Liu, W., Cai, Z., Han, B., Qian, T. et al. (2016). An overview of preparation and applications of stabilized zero-valent iron nanoparticles for soil and groundwater remediation. *Water Research, 100,* 245–266. DOI 10.1016/j.watres.2016.05.019.

18. Madaffari, M. G., Bilardi, S., Calabro, P. S., Moraci, N. (2017). Nickel removal by zero valent iron/lapillus mixtures in column systems. *Soils and Foundations, 57(5),* 745–759 DOI 10.1016/j.sandf.2017.08.006.
19. Sriram, G., Kigga, M., Uthappa, U. T., Rego, R. M., Kurkuri, M. D. (2020). Naturally available diatomite and their surface modification for the removal of hazardous dye and metal ions: A review. *Advances in Colloid and Interface Science, 282,* 102198. DOI 10.1016/j.cis.2020.102198.
20. Molnar, A. (2011). Catalytic applications of amorphous alloys: Expectations, achievements, and disappointments. *Applied Surface Science, 257,* 8151–8164. DOI 10.1016/j.apsusc.2010.12.046.
21. Azuma, D., Ito, N., Ohta, M. (2020). Recent progress in Fe-based amorphous and nanocrystalline soft magnetic materials. *Applied Surface Science, 501,* 166373. DOI 10.1039/C5RA02870A.
22. Tang, Y., Shao, Y., Chen, N., Liu, X., Yao, K. F. (2015). Insight into the high reactivity of commercial Fe-Si-B amorphous zero-valent iron in degrading azo dye solutions. *RSC Advances, 5(45),* 34032–34039. DOI 10.1039/C5RA02870A.
23. Yan, Y., Liang, X., Ma, J., Shen, J. (2020). Rapid removal of copper from wastewater by Fe-based amorphous alloy. *Intermetallics, 124,* 106849. DOI 10.1016/j.intermet.2020.106849.
24. Cao, C. R., Lu, Y. M., Bai, H. Y., Wang, W. H. (2015). High surface mobility and fast surface enhanced crystallization of metallic glass. *Applied Physics Letters, 107(14),* 577. DOI 10.1063/1.4933036.
25. Chen, F., Lam, C. H., Tsui, O. K. C. (2014). The surface mobility of glasses. *Science, 343,* 975–976. DOI 10.1126/science.1248113.
26. Brian, C. W., Yu, L. (2013). Surface self-diffusion of organic glasses. *Journal of Physical Chemistry A, 117(50),* 13303–13309. DOI 10.1021/jp404944s.
27. Soil environmental quality risk control standard for soil contamination of development land GB36600 (2018). http://www.mee.gov.cn/ywgz/fgbz/bz/bzwb/trhj/201807/t20180703_446027.shtml.
28. Li, X. H., Tang, Z. L., Chu, F. Y. (2009). Transfer behavior of heavy metals in soil around Cu-Ni mining area in Jinchang. *Journal of Jilin University, 1,* 131–136. DOI 10.3969/j.issn.1671-5888.2009.01.020.
29. Shaaban, M., Wu, Y., Peng, Q., Wu, L., Hu, R. (2018). The interactive effects of dolomite application and straw incorporation on soil N_2O emissions: Nitrous oxide emissions from an acidic soil. *European Journal of Soil Ence, 69,* 505–511. DOI 10.1111/ejss.12541.
30. Vasarevičius, S., Danila, V., Paliulis, D. (2019). Application of stabilized nano zero valent iron particles for immobilization of available Cd^{2+}, Cu^{2+}, Ni^{2+}, and Pb^{2+} ions in soil. *International Journal of Environmental Research, 13,* 465–474. DOI 10.1007/s41742-019-00187-8.
31. Kumpiene, J., Lagerkvist, A., Maurice, C. (2008). Stabilization of As, Cr, Cu, Pb and Zn in soil using amendments–A review. *Waste Management, 28(1),* 215–225. DOI 10.1016/j.wasman.2006.12.012.
32. Ure, A. M., Quevauviller, P., Muntau, H., Griepink, B. (1993). Speciation of heavy metals in soils and sediments. an account of the improvement and harmonization of extraction techniques undertaken under the auspices of the BCR of the commission of the european communities. *International Journal of Environmental Analytical Chemistry, 51(1),* 135–151. DOI 10.1080/03067319308027619.
33. Guan, X., Yang, H., Sun, Y., Qiao, J. (2019). Enhanced immobilization of chromium (VI) in soil using sulfidated zero-valent iron. *Chemosphere, 228,* 370–376. DOI 10.1016/j.chemosphere.2019.04.132.
34. Chen, F. L., Zhang, M. J., Ma, Q., Li, X. F., Wang, S. J. et al. (2013). Characteristics of $\delta^{18}O$ in precipitation and water vapor sources in lanzhou city and its surrounding area. *Environmental Science, 34,* 3755–3763. DOI 10.13227/j.hjkx.2013.10.020.
35. Mohan, V. B., Jayaraman, K., Bhattacharyya, D. (2020). Brunauer–Emmett–Teller (BET) specific surface area analysis of different graphene materials: A comparison to their structural regularity and electrical properties. *Solid State Communications, 320,* 114004. DOI 10.1016/j.ssc.2020.114004.
36. Wang, P., Wang, J. Q., Li, H., Yang, H., Huo, J. et al. (2017). Fast decolorization of azo dyes in both alkaline and acidic solutions by Al-based metallic glasses. *Journal of Alloys and Compounds, 701,* 759–767. DOI 10.1016/j.jallcom.2017.01.168.
37. Tong, X., Wang, G., Stachurski, Z. H., BednarÍk, J., Mattern, N. et al. (2016). Structural evolution and strength change of a metallic glass at different temperatures. *Scientific Reports, 6,* 386–474. DOI 10.1038/srep30876.

38. Chen, J., Zhu, L. (2007). Heterogeneous UV-fenton catalytic degradation of dyestuff in water with hydroxyl-Fe pillared bentonite. *Catalysis Today, 126(3),* 463–470. DOI 10.1016/j.cattod.2007.06.022.
39. Lien, H. L., Zhang, W. X. (2007). Nanoscale Pd/Fe bimetallic particles: Catalytic effects of palladium on hydrodechlorination. *Applied Catalysis B Environmental, 77(1),* 110–116. DOI 10.1016/j.apcatb.2007.07.014.
40. Phuengprasop, T., Sittiwong, J., Unob, F. (2011). Removal of heavy metal ions by iron oxide coated sewage sludge. *Journal of Hazardous Materials, 186,* 502–507. DOI 10.1016/j.jhazmat.2010.11.065.
41. Cao, C., Huang, K., Shi, J., Zheng, D., Zheng, D. N. et al. (2019). Liquid-like behaviours of metallic glassy nanoparticles at room temperature. *Nature Communications, 10(1),* 1–8. DOI 10.1038/s41467-019-09895-3.
42. Su, H., Fang, Z., Tsang, P. E., Zheng, L., Zhao, D. (2016). Remediation of hexavalent chromium contaminated soil by biochar-supported zero-valent iron nanoparticles. *Journal of Hazardous Materials, 318*, 533–540. DOI 10.1016/j.jhazmat.2016.07.039.